Dynamic organization of bacterial chromatin by DNA bridging proteins
Qin, L.

Citation
Qin, L. (2020, September 22). *Dynamic organization of bacterial chromatin by DNA bridging proteins*. Retrieved from https://hdl.handle.net/1887/136909

Cover Page

Universiteit Leiden

The handle http://hdl.handle.net/1887/136909 holds various files of this Leiden University dissertation.

Author: Qin, L.
Title: Dynamic organization of bacterial chromatin by DNA bridging proteins
Issue Date: 2020-09-22

Chapter 3

Mechanism of anti-repression of *Pseudomonas aeruginosa* H-NS family protein MvaT by the phage protein Mip

In this chapter, Fredj Ben Bdira performed and analyzed NMR experiments and performed molecular modelling. Nicholas Bowring performed and analyzed some of the TPM experiments and his-tag pull down assay.

Abstract

Bacteria and their associated bacteriophages are in a continuous battle, co-evolving defense and offense mechanisms. Bacterial xenogeneic silencers, H-NS family proteins, play important roles in bacterial phage defense and evolution by silencing incoming genes and genes acquired through horizontal gene transfer. The *Pseudomonas* phage LUZ24 encodes the Mip protein which binds the H-NS family protein MvaT of *Pseudomonas aeruginosa.* Binding of Mip was proposed to inhibit the silencing of phage LUZ24 DNA by MvaT. However, the mechanism by which Mip modulates MvaT function remains unclear. In this study we investigated how the DNA binding properties of MvaT are affected by Mip. Also, we defined how Mip interacts with MvaT and how this translates into altered DNA structuring properties. Our studies reveal that Mip interferes with the formation and stability of the bridged MvaT-DNA complex. This effect is due to interaction of Mip with both the dimerization and the DNA-binding domain of MvaT. Based on these observations we propose that binding of Mip promotes the half open - bridging incompetent - state of MvaT, resulting in relief of MvaT-mediated gene silencing.

Introduction

Bacteriophages - viruses infecting bacteria - are among the most abundant and diverse organisms on earth [1,2], found wherever bacteria exist, and they represent a constant challenge to bacteria. Bacteria and their associated bacteriophages co-evolve in a continuous battle, developing defensive and offensive strategies [3-5]. To protect themselves against bacteriophages, bacteria have evolved a variety of defense mechanisms, encoded in their genomes, including restriction modification [6], CRISPR-Cas [7] and xenogeneic silencing systems [8]. Bacterial xenogeneic silencers play important roles in bacterial evolution by recognizing and silencing foreign genes acquired through horizontal gene transfer [9,10], resulting from transformation, conjugation or transduction. The silencing of these foreign genes up to the moment that their expression is induced following an environmental cue can provide bacteria with a competitive advantage under specific conditions without compromising the integrity of global genome regulation [11]. Four types of bacterial xenogeneic silencers have been identified to date. These proteins all belong to the family of H-NS like proteins, defined by their functional similarity to the H-NS protein (see Chapter 1) [8,12-14]. Members include H-NS of *Proteobacteria* [15], MvaT of *Pseudomonas species* [16], Lsr2 of *Actinomycetes* [17] and Rok of *Bacillus species* [18]. The gene silencing mechanism of H-NS like proteins is determined by their ability to bind and spread across genes. Characteristic of H-NS family proteins is the formation of nucleofilaments along the DNA and protein-mediated DNA-DNA bridges (see Chapter 4) [19-22]. In response to bacterial xenogeneic silencing systems, bacteriophages have evolved resistance mechanisms by encoding proteins antagonizing H-NS silencing. For instance, the Gp5.5 protein of *E. coli* phage T7 is able to counteract H-NS activity in *E. coli* upon phage infection [23]. Gp5.5 binds to the central oligomerization domain of H-NS and disrupts higher-order H-NS-DNA complexes, leading to counter-silencing of genes controlled by H-NS [24,25]. Another example is the Arn protein of *E. coli* phage T4, which is a DNA mimic, which has been proposed to counteract H-NS mediated repression by targeting its DNA binding domain and thus interfering with DNA binding [26]. Bacteriophage Mu employs yet another mechanism. Binding of IHF to its site upstream of the early promoter (Pe) interferes with the formation of H-NS-DNA complexes and counteracts the H-NS-mediated repression of this promoter [27,28]. The EPV1 phage encodes H-NS on its genome, which

was proposed to repress expression of genes involved in host defense mechanisms against phage infection such as CRISPR associated proteins and a Type III restriction-modification system [29]. However, insights into the precise molecular mechanisms of inhibition are generally lacking.

The H-NS family protein MvaT of *Pseudomonas aeruginosa* plays an important role in genome organization and gene repression [16]. The *Pseudomonas* phage LUZ24 (and several related phages) encode the Mip (MvaT inhibiting protein) which binds MvaT and modulates its function. The Mip protein is one of the early phage genes expressed directly following host infection. Based on evidence that it inhibits DNA binding of MvaT, it was proposed that Mip inhibits the silencing of phage LUZ24 DNA by MvaT [30]. A number of possible mechanisms for modulation of MvaT function can be envisioned based on the nucleation-propagation-bridging assembly pathway of MvaT-DNA complexes (see Chapter 2) [13,19]. Mip may either alter 1) the DNA binding affinity of MvaT, which is important for protomer binding, 2) the multimerization properties of MvaT which determine the cooperativity of nucleoprotein filament formation or 3) the ability of MvaT to bridge DNA. In this study we investigated which of these steps in the assembly of the bridged complex is affected by Mip. Moreover, we defined how Mip interacts with MvaT and how this translates into altered DNA structuring properties. Based on this information we propose a mechanism by which Mip relieves MvaT-mediated silencing of phage genes.

Results

Mip cannot inhibit DNA binding of MvaT

It has been suggested that the Mip protein encoded on the *Pseudomonas* phage LUZ24 genome can inhibit the formation of MvaT-DNA complexes [30]. The underlying mechanism was proposed to be the inhibition of DNA binding by MvaT. However, support for such mechanism is minimal as MvaT has multiple modes of DNA binding (see introduction), which cannot be distinguished by gel electrophoresis as done in the study reporting the identification of Mip [30]. First, to verify the effect of Mip on the DNA binding of MvaT, we also performed electrophoretic mobility shift assay (EMSA). These experiments demonstrate that MvaT binds DNA (figure 3.1a), and that Mip alone does not bind to the DNA (figure 3.1b). Addition of increasing amounts of Mip from 1 to 10 μM, does not inhibit the formation of an MvaT-DNA complex (figure 3.1d), which is different from the results reported earlier [30]. To validate our observations, we next examined the effect of

Mip on the DNA binding of MvaT F36D/M44D, an MvaT mutant, that does not oligomerize and exists exclusively as dimer (see Chapter 2) [13]. Similar to MvaT wt, the DNA binding of MvaT F36DM44D was not inhibited by adding increasing amounts of Mip (figure 3.1c and 3.1e). Rather than inhibition, in both cases (figure 3.2d and 3.2e) complexes with further reduced mobility are observed upon introduction of Mip.
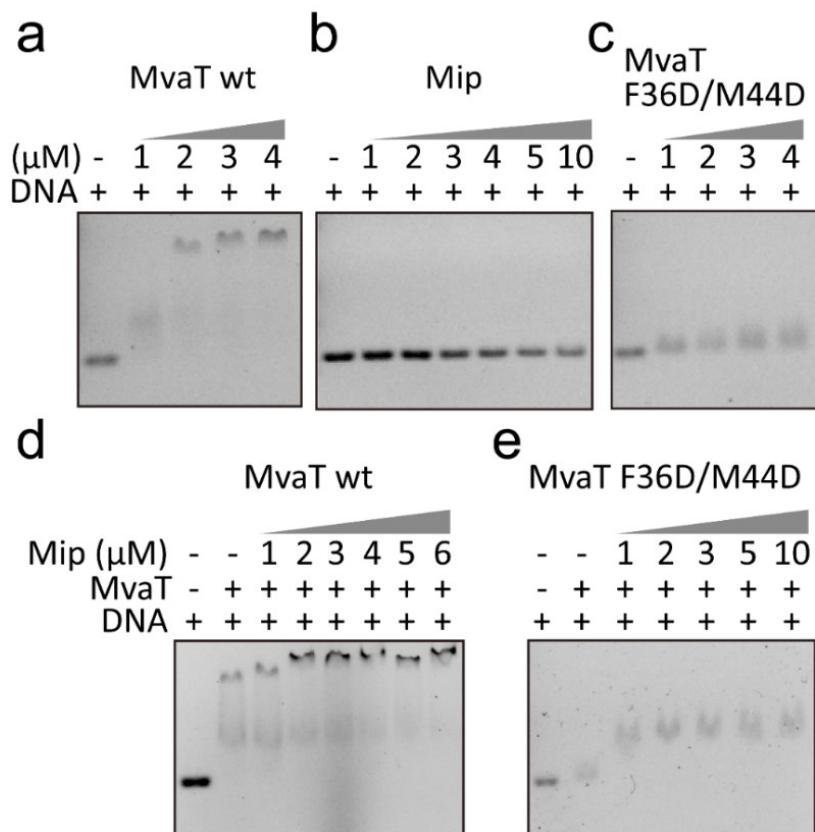

Figure 3.1. **Mip does not inhibit DNA binding of MvaT**. a) Gel electrophoretic mobility shift assay showing DNA and its binding by MvaT at concentrations of 1, 2, 3, and 4 μM. b) Gel electrophoretic mobility shift assay showing DNA and its binding by Mip at concentrations of 1, 2, 3, 4, 5, and 10 μM. c) Gel electrophoretic mobility shift assay showing DNA and its binding by MvaT F36DM44D at concentrations of 1, 2, 3, and 4 μM. Gel electrophoretic mobility shift assay showing DNA binding by d) 2 μM MvaT and e) 5 μM MvaT F36D/M44D, and the titration of the MvaT-DNA complexes with Mip at various concentrations as indicated in figure.

Mip cannot inhibit lateral MvaT-DNA complex formation

Oligomerization of MvaT is required for the formation of nucleoprotein filaments along DNA, and is essential for the function of MvaT in gene silencing [20,31]. As in our hands Mip does not inhibit

binding of MvaT to DNA, the effect of Mip on MvaT might be due to altered oligomerization behavior of MvaT along DNA. To investigate this possibility, we investigated the formation of MvaT nucleoprotein filaments and the effect of Mip on this process using Tethered Particle Motion (TPM) (see Chapter 2) [13,19]. DNA compaction, indicated by a reduction in RMS, was observed at low concentration of MvaT (figure 3.2, see Chapter 2) [13]. We attributed this effect to bending of DNA by individually bound MvaT dimers. Upon addition of increasing amounts of MvaT, the DNA was stiffened, indicated by an increase in RMS, reaching saturation level at 1200 nM. Mip alone did not alter the RMS in line with our observations that it does not bind to DNA (figure 3.1b).
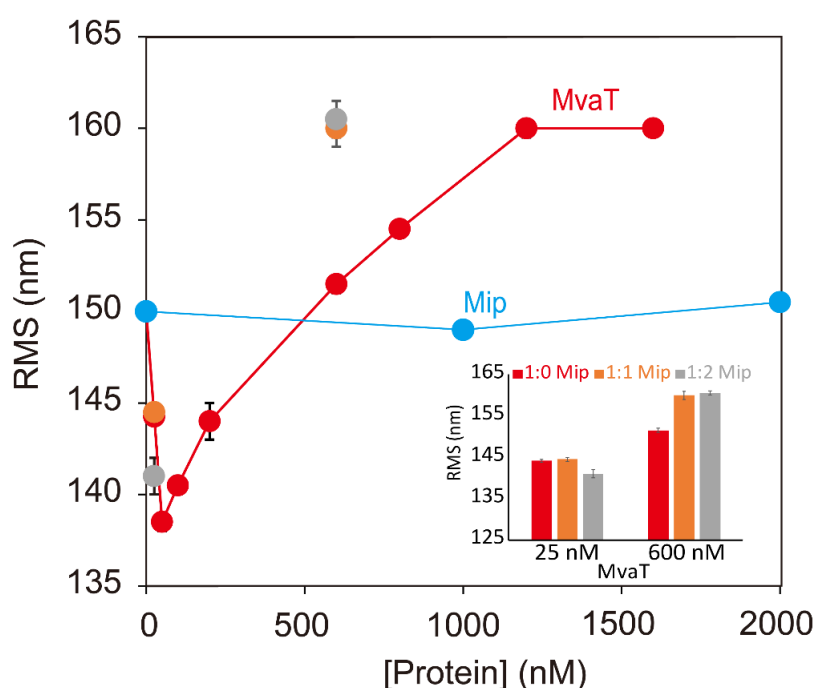

Figure 3.2. **Modulation of MvaT DNA-binding activity by Mip**. The curve (red in color) represents the RMS of DNA bound by MvaT at concentrations from 0 to 1600 nM as measured using the Tethered Particle Motion assay in the absence of Mip. The curve (blue in color) represents the RMS of DNA bound by Mip at concentrations from 0 to 2000 nM as measured using the Tethered Particle Motion assay in the absence of MvaT. The histogram indicates RMS values obtained at fixed concentrations of MvaT (25 nM and 600 nM) with varying amounts of Mip added. In the main plot, the TPM results of Mip effect on the DNA binding of MvaT at 1:1 and 1:2 ratio are indicated with orange and grey dots, respectively. The error bars represent the standard deviation of at least duplicate and some are hidden behind the data points.

To test whether Mip has an effect on the formation of the MvaT DNA filament, TPM was performed with fixed MvaT concentrations of 25 nM and 600 nM, with varying amounts of Mip added. At 25 nM MvaT addition of Mip has no or a very mild effect on the RMS of the MvaT-DNA complex. As the RMS does not return to bare DNA levels, these observations suggest that Mip does not inhibit DNA binding by MvaT in line with our observations reported in figure 3.1d. Also, at 600 nM the MvaT-DNA nucleoprotein filament is not perturbed by Mip. The increase in RMS indicates that Mip and MvaT bound together lead to a more extended nucleoprotein filament. This observation implies that Mip does not interfere with oligomerization of MvaT along DNA.

Mip interferes with the formation and stability of MvaT-DNA bridging complexes

MvaT is capable of forming nucleofilaments along DNA (see Chapter 2) [13,20] and protein-DNA bridging complexes (see Chapter 2) [13,20,32]. The DNA binding properties of MvaT are affected by the phage anti-MvaT protein Mip, while DNA binding of MvaT is not inhibited by Mip. To determine whether Mip affects the ability of MvaT to bridge DNA, we used the protein-DNA bridging assay established in earlier work (see Chapter 5) [19,33]. MvaT was found to be able to bridge DNA in the presence of divalent salt or monovalent salt at high concentration (see Chapter 2) [13]. Here we performed the experiments in the presence of $MgCl_2$. In this assay a fixed amount of MvaT (2.4 µM) is used which yields a 35% recovery of DNA in the absence of Mip. The DNA recovery decreases upon addition of increasing amounts of Mip up to 3.6 µM (figure 3.3a). Maximum inhibition of DNA recovery occurs at a Mip concentration of 1.2 µM where the Mip : MvaT molar ratio is 0.5 (figure 3.3a). Experiments carried out using an alternative divalent anion, Ca^{2+}, confirm efficient DNA bridging by MvaT, as well as perturbation of MvaT-mediated DNA bridging by Mip (figure S3.1). Our results thus clearly demonstrate that Mip interferes with the formation of bridged MvaT-DNA complexes. Next, to examine whether Mip has an effect on existing bridged MvaT-DNA complexes, we carried out a variation on the DNA bridging assay in which DNA recovery is measured over time following addition of Mip (MvaT:Mip = 1:1) at different time points during bridged MvaT-DNA complex assembly (figure 3.3c). As a control, we measured the DNA recovery promoted by MvaT over time without adding Mip. In this case DNA recovery increases over time and reaches saturation at t = ~ 600 s (figure 3.3b). When Mip is introduced at the beginning (t = 0 s), a minimal increase of DNA recovery was observed over time (up to 5%).

This observation indicates that Mip interferes with the assembly of the bridged MvaT-DNA complex. When Mip is introduced when bridged MvaT-DNA complex formation has progressed for 180 s (but has not reached saturation levels) and 1200 s (has reached saturation levels), reduction in DNA recovery is observed. This demonstrates that bridged MvaT-DNA complexes can be perturbed by Mip. Taken together, our results demonstrate that the phage protein Mip can not only interfere with the formation of bridged MvaT-DNA complexes, but also perturbs pre-assembled bridged MvaT-DNA complexes.
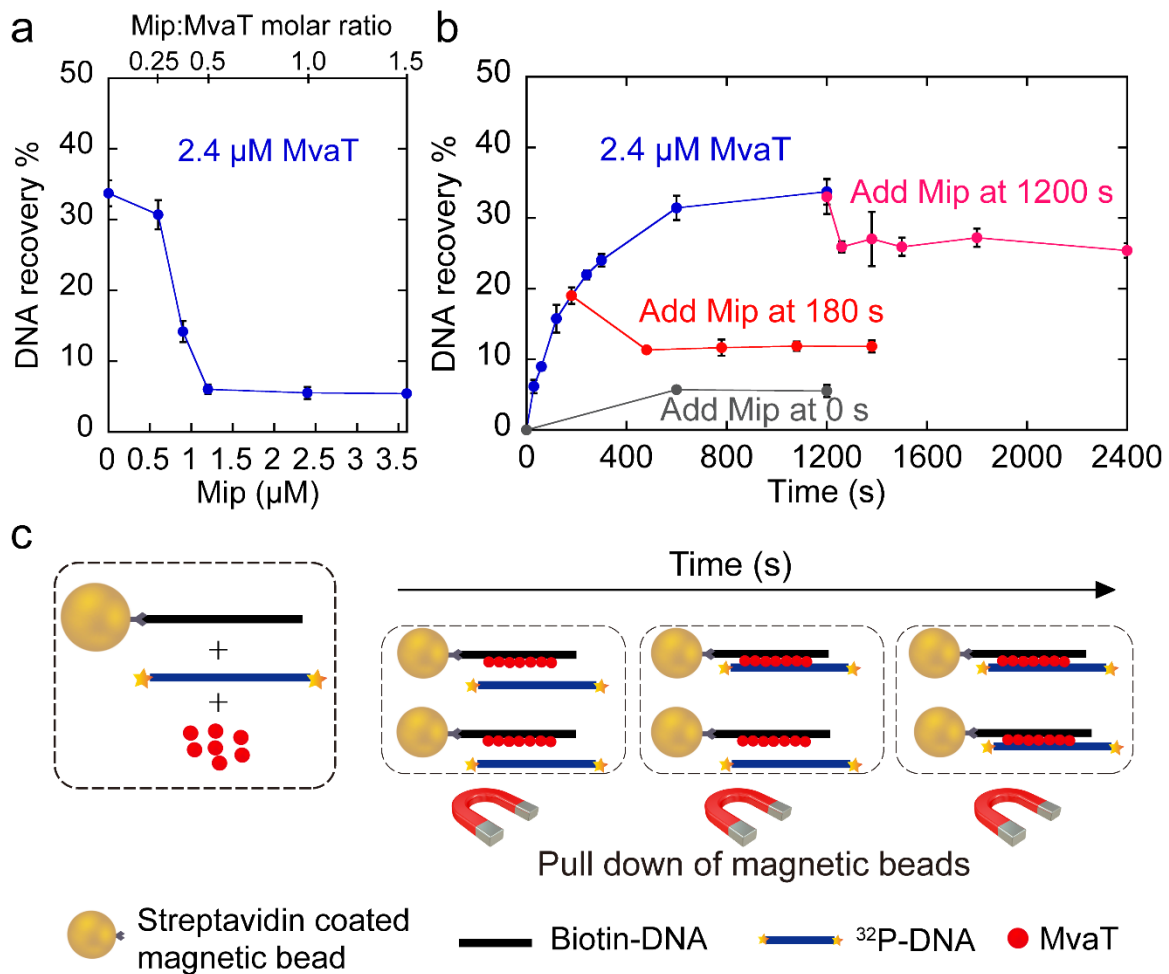

Figure 3.3. **Mip inhibits the formation of bridged MvaT-DNA complexes and perturbs existing bridged MvaT-DNA complexes.** a) Mip inhibits the formation of the bridged MvaT-DNA complex. DNA bridging efficiency (as a percentage of the input DNA) in presence of MvaT (2.4 µM), as affected by titration of Mip at concentrations up to 3.6 µM. b) Mip perturbs existing bridged DNA-MvaT-DNA complexes. The blue curve represents the kinetics of MvaT-DNA bridge formation without adding Mip. The red and pink curve represent the kinetics of MvaT-DNA bridge formation with Mip introduced at 180 s and 1200 s respectively. The grey

curve represents Mip introduced at the beginning (t = 0 s). Data are plotted as mean values and the error bars represent the standard deviation from at least 2 independent measurements. c) Experimental schematic of bridging assay over time. Magnetic beads connect to biotin labeled DNA; radioactive labeled DNA was bridged by adding MvaT; at various time points, the bridging reactions were terminated by magnetic pull down and buffer washing of beads. If required, Mip (MvaT:Mip = 1:1) was added at different time points to measure the effect of Mip on the formation of MvaT-DNA bridge complexes over time.

Mip binds the N-terminal domain of MvaT

The fold architecture of the MvaT monomer consists of an α-helical N-terminal oligomerization domain (residues 1-64) tethered to a C-terminal DNA binding domain (DBD) (residues 79-124) by a flexible linker (residues 65-78) (figure 3.4a). The structural unit of MvaT nucleofilaments is a dimer (protomer) formed by "coiled-coil" interactions between the first N-terminal α-helices of two MvaT monomers (α1: residues 1-32), dimerization site 1 (figure 3.4a). The MvaT protomers form high-order oligomers through a second dimerization site, site 2 (α2: residues 50-58). Both coiled-coils are formed by a hydrophobic core and stabilized by salt bridges (see Chapter 2) [13].

Above we have shown that the inhibitory effect of Mip on the DNA bridging activity of MvaT, is neither due to inhibition of DNA binding by MvaT nor to inhibition of oligomerization of MvaT along DNA. To define the mechanism underlying the inhibitory function of Mip, we investigated how Mip binds to MvaT. Previously, it was suggested that Mip binds to the MvaT oligomerization domain and linker region (residues 1–80) [30]. To substantiate these suggestions, here we investigated the interaction of Mip with both the N-terminal domain (residues 1-62) and the DBD (residues 79-124) of MvaT in a magnetic bead pull down assay. The results of this assay confirm that Mip binds to the N-terminal domain (residues 1-62) (figure 3.4a) and not to the DBD (residues 79-124), and also suggest that the linker region (65-80) may not be required for the Mip-MvaT complex formation.

To determine the stoichiometry of the protein-protein complex and the affinity between the two proteins, we performed isothermal titration calorimetry (ITC) of the MvaT dimer (F36D/M44D) titrated with Mip. The fit of the titration data to a 1:1 binding model yields a K_D of 170 $\pm$ 14 nM with a number of binding sites N= 0.56 (figure 3.4c). These results suggest a tight binding between the

two proteins with a stoichiometry of 1:2. Thus, the Mip-MvaT complex appears to be formed by the interaction of one molecule of Mip with two molecules of MvaT.
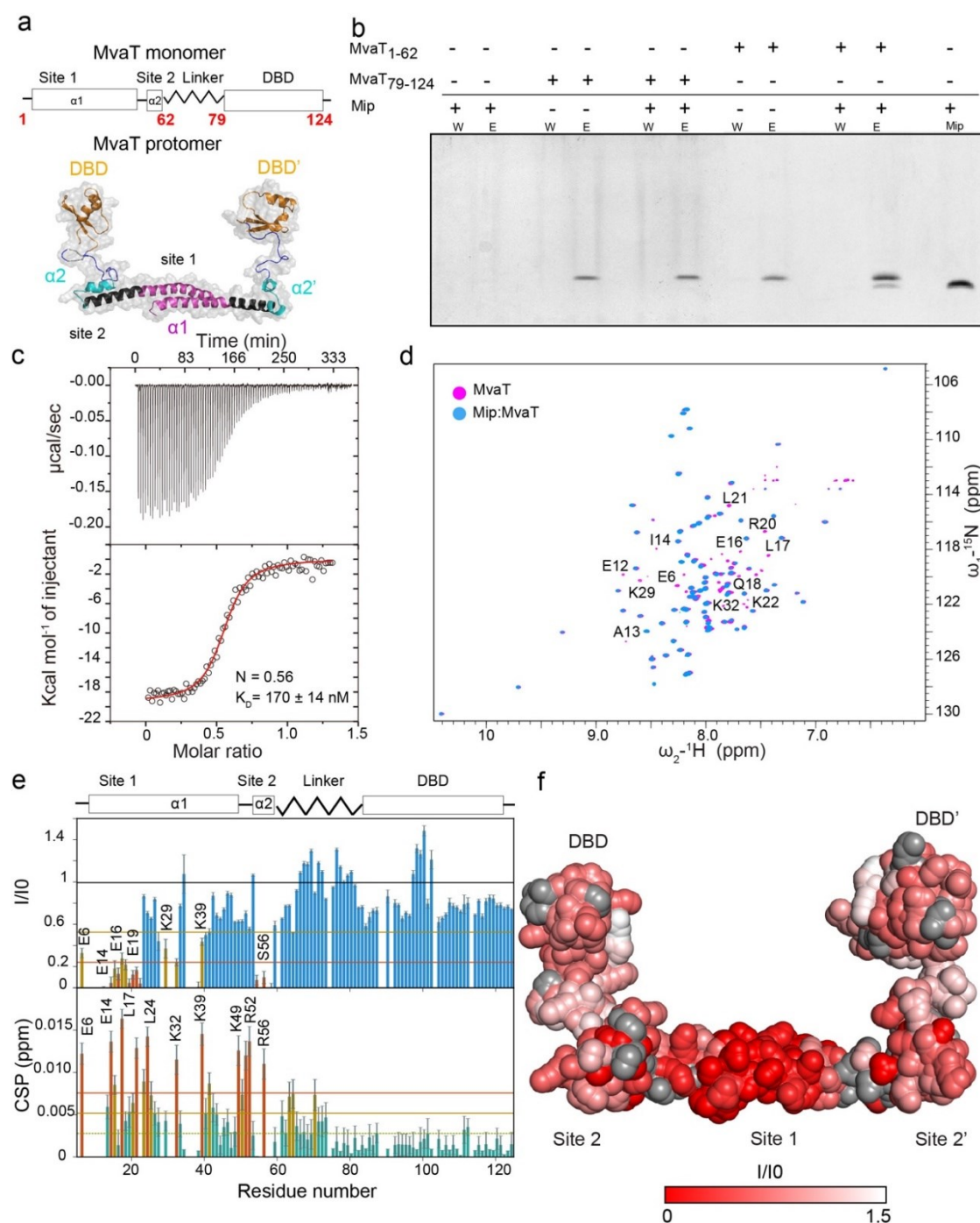

Figure 3.4. **Mip interacts with the N-terminal domain of MvaT.** a) MvaT monomer and protomer fold topology. In the lower panel is the structural model of the MvaT protomer adopted from (see Chapter 2) [13]. (b) Tricine gel analysis of the his-tag pull down assay. His-tagged MvaT truncates captured on magnetic beads were incubated with Mip. A Mip reference marker was used to identify Mip. c) ITC titration of Mip (230

μM) into MvaT (16 μM) using 2 μl of injection volume. The red line represents the best fit plot by using a 1:1 binding model. The fitting yields a K_D = 170 ± 14 nM and N = 0.56 sites. (b) Overlay between MvaT dimer ^{15}N-^{1}H HSQC spectra in the free state (magenta) and at 1.2 Mip:MvaT molar ratio (blue). Amide resonances which experience severe line broadening upon titration with Mip are labelled. (e) The upper panel depicts the ^{15}N-^{1}H HSQC spectra peak intensities ratio of MvaT in the presence of 1.2 molar ratio of Mip (I) and in the free state (I0) versus the protein residue number. Lower panel shows weighted average CSP of the MvaT resonances between the same points of titration. Resonances with CSP more than two (orange line) or one (yellow line) standard deviation (SD) from the 10% trimmed mean (green dashed line) are labelled and shown in orange, yellow and green bars, respectively. (f) Mapping of the residues with reduction in their peak intensities (red/white gradient), upon addition of Mip, on the MvaT dimer structural model surface. Residues with no data are colored in grey spheres.

As the used MvaT variant (F36D/M44D) can only form a dimer through the interaction between the two N-terminal α-helices (site1), we hypothesize that Mip is mainly interacting with site 1, to satisfy the stoichiometry of the complex. To corroborate this hypothesis, we performed a NMR titration of the MvaT dimer (F36D/M44D) with Mip using the same experimental conditions as used for the ITC titration. The ^{15}N-^{1}H HSQC spectrum of MvaT dimer was previously assigned (see Chapter 2) [13], enabling the identification of the exact region on the dimer to which Mip binds.

The addition of Mip to MvaT induced a decrease in the intensity of multiple resonances in the protein spectrum with minor changes in their chemical shift positions (figure 3.4d). Such effect is typical of a strong binding, in agreement with the ITC results (K_D= 170 ± 14 nM). At 1.2 molar ratio, the ratio between the peak's intensities of the MvaT free and bound to Mip shows that the resonances affected significantly are for residues located in the dimerization site 1 (residues 1-22) (figure 3.4e and 3.4f). A general yet non-uniform line broadening is also observed for amide resonances of the linker and the DBD (figure 3.4e). This observation might be in part explained by the increase in the rotational correlation time (τ_c) of the MvaT dimer upon complex formation with Mip. In addition, we propose that intermolecular interactions arise between Mip and MvaT DBD and linker region. These interactions are possibly too weak to be probed by the pull-down assay or ITC.

Previously we have found that at low ionic strength, the MvaT dimer exhibits intramolecular electrostatic interactions between its oppositely changed N-terminal and DBD domains, which are further stabilized by the linker region. These interactions cause line broadening in the amide's resonances of the DBD and linker. Increase in ionic strength destabilizes these intramolecular interactions and thus induces an enhancement of the peak intensities of the backbone amides of the DBD and linker (see Chapter 2) [13]. The NMR titration of MvaT with Mip was performed at high ionic strength (50 mM KCl, 16 mM MgCl$_2$), therefore it is expected that the line broadening due to electrostatic interactions between the oppositely charged domains is negligible. Therefore, we propose that the observed non-uniform lines broadening of the resonances of the residues of the linker and DBD, in the presence of Mip, is due to the formation of new intermolecular interactions between these regions and Mip.

Modeling of the Mip-MvaT complex

To understand the mechanism by which Mip modulates the DNA binding properties of MvaT we generated a molecular model of the Mip-MvaT$_2$ complex. Mip is a 46 amino acids basic protein with no tertiary structure available. The secondary structure of the Mip polypeptide chain was predicted to consist of an N-terminal (α1) and C-terminal (α2) helix connected by a flexible loop (figure 3.5a).

Next, we performed *ab initio* modelling using Rosetta [34] to predict the 3D structure of Mip. In the best structure, the two helices of Mip form a "coiled coil" motif with a hydrophobic core stabilized by a salt bridge (figure 3.5a and 3.5b). The structural models of the MvaT dimer and Mip were used to perform restrained docking with HADDOCK [35] using the NMR titration data as experimental restraints. In our modelling we only considered the binding of Mip to the MvaT dimer N-terminal domain (residues 1-22), as it appears to represent the primary interaction site between the two proteins (K$_D$ =170 $\pm$ 14 nM). Multiple structures of the Mip-MvaT$_2$ complex were obtained (figure S3.2 and M&M). The lowest energy structure of the complex is shown in figure 3.5c. The complex of the two proteins seems to be formed by electrostatic interactions between the surfaces of the positively charged Mip and the negatively charged site 1 of the MvaT dimer (figure 3.5c and 3.5d).
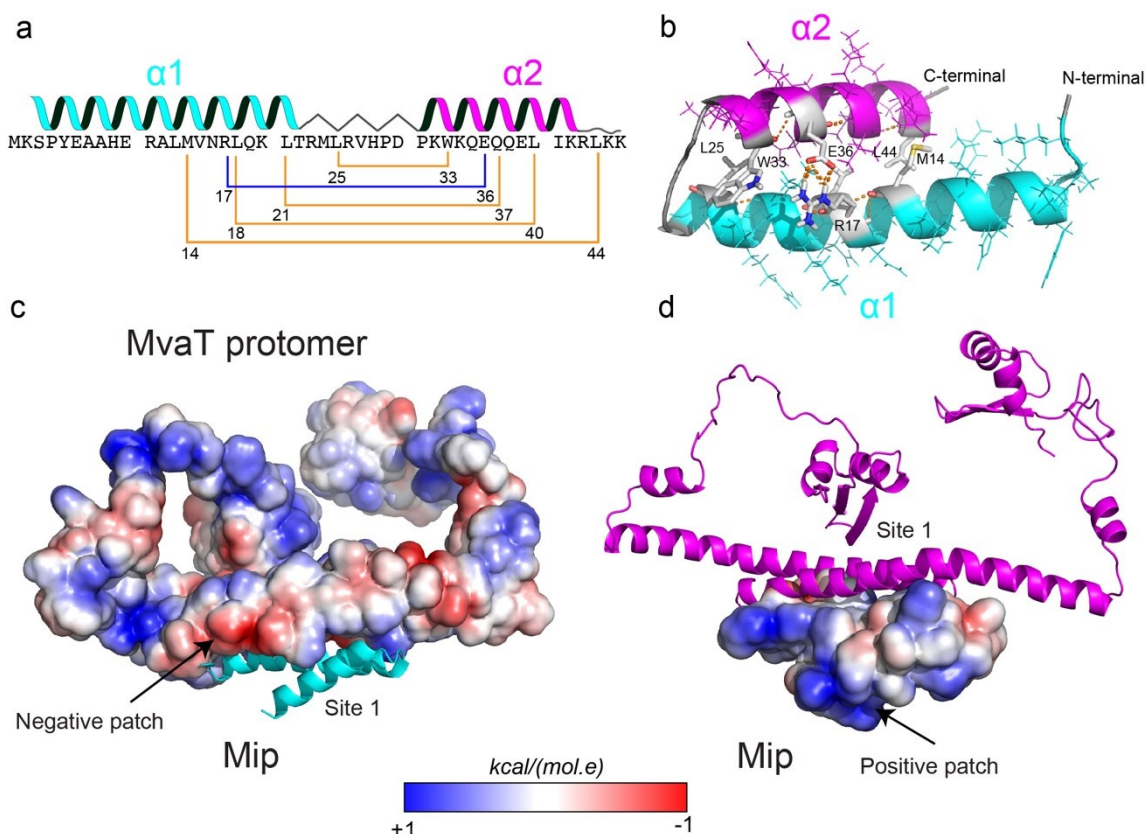
Figure 3.5. **Mip-MvaT protein complex model.** a) Mip secondary structure predicted by JPred 4 server [36]. The N-terminal helix (α1) is shown in cyan and the C-terminal helix (α2) is in magenta. (b) The lowest energy structure obtained from the *ab initio* Rosetta modeling [34]. The side chains of the residues involved in the hydrophobic core of the coiled coil are shown in stick and labelled. The hydrophobic interactions are shown in (a) with yellow line and the salt bridge is shown in blue. The color code is as in (a). (c) and (d) The HADDOCK best structure of the Mip-MvaT$_2$ complex (see M&M) with the electrostatic potential surfaces of MvaT protomer and Mip, respectively.

How can our findings be structurally rationalized?

The TPM results indicate that Mip binding affects the stiffening and degree of compaction (due to bending) of DNA by MvaT. Our results show also that binding of Mip to the central dimerization domain of MvaT (site 1) can inhibit its DNA bridging activity, while DNA stiffening is not inhibited. This indicates that in the presence of Mip, despite the formation of MvaT nucleofilaments along the DNA, these filaments are unable to interact with a second DNA duplex to form a bridge. This situation resembles the low salt condition described in earlier work (see Chapter 2) [13] in which MvaT protomers adopt a half open state, in which one of the DBD's is

sequestered by intramolecular electrostatic interaction with site 1. An increase in ionic strength destabilizes these interactions and the MvaT protomers expose both of their DBD's, adopting fully open states, able to bridge two DNA duplexes (see Chapter 2) [13]. Therefore, we hypothesize that Mip counteracts the effect of the high ionic strength, used in the bridging assay condition (50 mM KCl, 16 mM MgCl$_2$), on the MvaT conformational landscape and shifts the structural equilibrium towards the half open state, similar to the low salt condition (50 mM KCl, in the absence of MgCl$_2$). This is supported by the NMR titration data which indicate that intermolecular interactions between Mip and the DBD exist. Therefore, in the presence of Mip and at high ionic strength MvaT protomers adopt a half open state that is able to stiffen, but not to bridge DNA. Further structural studies are required to validate this model.
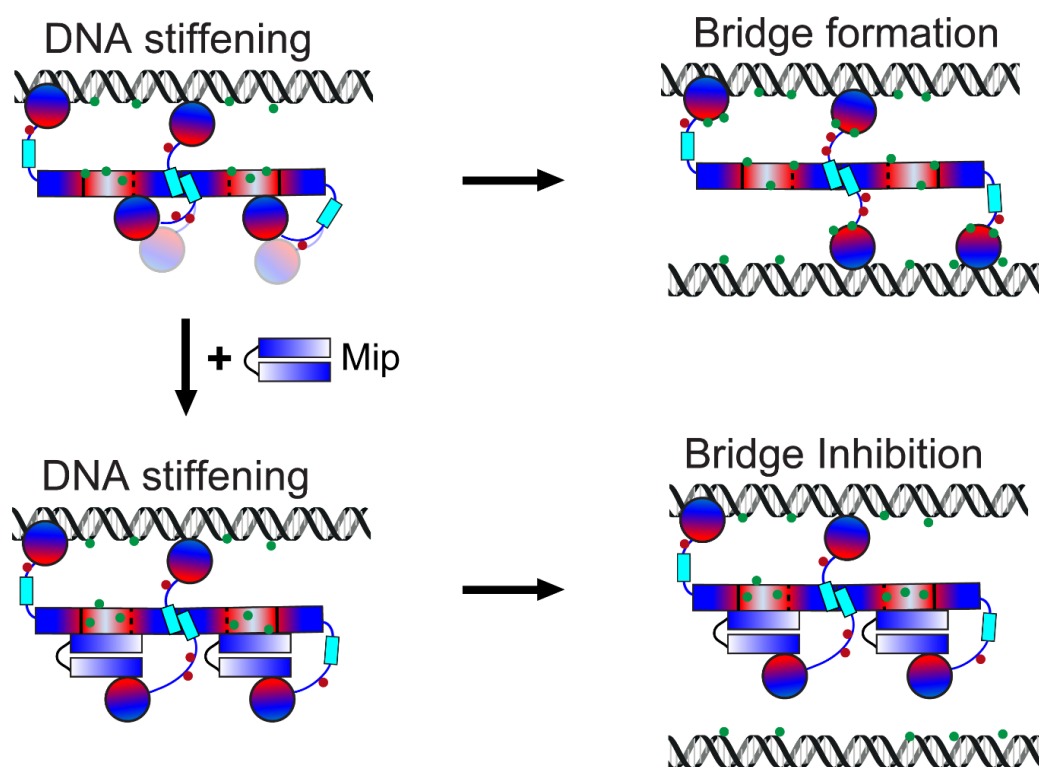

Figure 3.6. **Proposed mechanism for inhibition of MvaT DNA bridging activity by Mip.** The electrostatic surfaces of MvaT dimer and Mip are shown schematically in a red (negative)/white (neutral)/blue (positive) color gradient. Green and red dots are for ions (Mg^{2+}) and counter ions (Cl$^-$), respectively.

Discussion

In this work we have investigated the molecular mechanism by which the phage encoded Mip protein modulates MvaT activity. Mip interferes with the formation and maintenance of bridged MvaT-DNA complexes. This is a novel mechanism adding to the repertoire of distinct direct modulators of H-NS like protein activity [37,38]. Previously identified mechanisms involved interference with DNA binding (Arn) [26], multimerization (H-NST) [39] and stimulation of DNA bridging (Hha/YdgT) [19]. Hha/YdgT operates in strikingly similar manner as Mip: it associates with the central dimerization domain and exposes a charged surface facing outward, available for interaction with other partners. However, whereas Hha exposes a positively charged surface likely to interact with DNA and thus promoting DNA bridging, Mip exposes a positively charged surface, sequestering the DNA binding domain, shifting the structural equilibrium towards the half open state and disfavoring DNA bridging.

The interaction and co-evolution between a bacteriophage and its bacterial host play a key role in the ecological and evolutionary processes of microbial communities. Successful bacteriophage infection requires coping with bacterial resistance systems. One such bacterial resistance systems is that executed by H-NS-like proteins which cause xenogeneic silencing. To mitigate the effects of such H-NS-like proteins, bacteriophages encode proteins counteracting gene silencing by H-NS-like proteins. Our results show that the phage protein Mip is capable of inhibiting the DNA bridging activity of H-NS-like protein MvaT without inhibiting the DNA stiffening activity of the protein. DNA bridging is believed to be crucial in gene silencing [40,41]. To enhance the activity of H-NS proteins in gene silencing, bacteria themselves also encode proteins that modulate what type of H-NS-DNA complex is formed. Binding of Hha to H-NS exposes a positively charged surface [42] and stimulates its DNA bridging activity [19], which facilitates H-NS-mediated silencing of foreign genes in bacteria [43]. The Hha family protein YdgT also enhances DNA bridging [19]. YdgT, however, stimulates DNA bridging by enhancing the cooperativity of filament formation, the step preceding bridged H-NS-DNA complex formation [19].

In general, a better understanding of how viral proteins counteract H-NS proteins is important for design of proteins or molecules countering phage infection. Potential applications of such molecules can be envisioned in biotechnology, where phage infections are a threat to large

scale culturing, or in phage therapy where they may aid in enhancing the ability to infect and kill their host. Moreover, due to their global role in gene regulation in bacteria H-NS-like proteins are potential drug targets to mitigate bacterial infections. Understanding at the molecular mechanistic level how H-NS activity is modulated is key to such developments.

Materials and Methods

Construction of plasmids

The plasmids encoding MvaT of *P. aeruginosa* (pRD228), its derivatives (MvaT F36D/M44D (pRD277), MvaT 1-62-His (pRD360) and MvaT 79-124-His (pRD361)) and Mip of Pseudomonas phage LUZ24 (pRD232) were constructed using pET30b as vector by Gibson assembly [44]. The cloned sequences were verified by DNA sequencing.

DNA substrates

All tethered particle motion and bridging assay experiments were performed using a random, AT-rich, 685 bp (32% GC) DNA substrate used in previous research (see Chapter 2) [13,19]. The DNA substrate was generated by PCR and the products were purified using a GenElute PCR Clean-up kit (Sigma-Aldrich). If required, DNA was ^{32}P-labeled as described previously [19]. For the electrophoretic mobility shift assay an AT-rich 200 bp (31%GC) was generated using the same procedure.

Protein expression and purification

BL21 (DE3) pLysS cells transformed with (pRD228, pRD277, pRD360, pRD361 and pRD232) were grown in 2l of LB supplemented with kanamycin (100 µg/ml) at 37°C to an OD600 of ~0.6. Protein expression was induced with 0.5 mM isopropyl β-D-1-thiogalactopyranoside (IPTG) overnight at 18°C. Cells were centrifuged at 7000 × g for 15 min at 4°C. MvaT and MvaT F36D/M44D were purified as described previously (see Chapter 2) [13]. MvaT 1-62-His and MvaT 79-124-His were purified with modifications. The harvested cells were lysed by sonication in a lysis buffer containing 20 mM Tris-HCl (pH 8.0), 1 M NaCl. The lysate was cleared by centrifugation at 37 000 × g for 30 min at 4°C. Next, the supernatant was loaded on a HisTrap HP

5ml column (GE healthcare Life sciences) and the protein was eluted by applying an imidazole gradient from 0 to 1 M. The eluted fractions were checked by SDS-PAGE and the fractions that contain the target protein were pooled, concentrated and buffer exchanged using a PD10 column to 20 mM tris-HCl pH 7, 100 mM KCl. Next, the MvaT 1-62-His and MvaT 79-124-His were loaded on a HiTrap Q HP 5ml and HiTrap SP HP 5ml column (GE healthcare Life sciences) respectively and eluted by applying a NaCl gradient (from 0.1 to 1 M). The eluted fractions were also checked by SDS-PAGE and the pooled fractions were concentrated to a 500 µl volume with an Amicon 10 kDa cut-off filter. The concentrated protein fractions were loaded on a GE Superdex 75 10/300 GL column and eluted with 20 mM Tris-HCl pH 8, 300 mM KCl, 10% Glycerol. For the purification of Mip, the harvested cells were lysed by sonication in a lysis buffer containing 20 mM Tris-HCl (pH 7.0), 100 mM NaCl. Next, the supernatant was loaded on a HiTrap SP HP 5ml column (GE healthcare Life sciences) and the protein was eluted by applying a NaCl gradient from 0.1 to 1 M. The eluted fractions were checked by SDS-PAGE and the fractions that contain the target protein were pooled, concentrated and loaded into a GE Superdex 75 10/300 GL column and eluted with 20 mM Tris-HCl pH 8, 300 mM KCl, 10% Glycerol. The purity of the protein was checked by SDS-PAGE and the concentration was determined using a Pierce BCA protein assay kit (Thermo Scientific).

His-tag pull down assay

120 µl of the High-Density Nickel Agarose (Jena Bioscience) suspension was pipetted into an Eppendorf tube. The beads were prepared by changing the solution to binding buffer (100 mM NaCl, 10 mM tris-HCl pH 7.2, 50 mM imidazole, 20 mM $MgCl_2$). The nickel beads were then centrifuged at 7000 rpm for 2 minutes and the supernatant was removed. 250 µl of the desired combination of MvaT 79-124-His (40 µM), His-MvaT 1-62 (40 µM) and/or Mip (40 µM), in binding buffer, was added to the prepared nickel beads. This was incubated for 30 minutes while being shaken at 1000 rpm. After incubation the samples were centrifuged at 3000 rpm for 2 minutes. The supernatant was removed, and the pellet was carefully resuspended in 250 µl of binding buffer. This was referred to as a washing step and was repeated a total of six times. Following the final washing step, 250 µl of elution buffer (100 mM NaCl, 10 mM tris HCl pH 7.2, 1.5 M imidazole, 20 mM $MgCl_2$) was added to the beads instead of binding buffer to elute any protein bound to the

bead. The samples were centrifuged at 3000 rpm for 2 minutes and the supernatant was collected. 10 µl of the supernatant was run on a tricine gel.

Tethered Particle Motion

Tethered Particle Motion experiments were performed as described previously (see Chapter 2) [13] and the flow cells were prepared with minor modifications. In short, first, the flow cell was washed with 100 ml of wash buffer (10 mM Tris-HCl pH 8, 150 mM NaCl, 1 mM EDTA, 1 mM DTT, 3% Glycerol, 100 µg/ml BSA (ac)) and experimental buffer (10 mM Tris pH 8, 50 mM KCl, 10 mM EDTA, 5% glycerol). The flow cell was sealed after adding protein (MvaT alone or MvaT-Mip mixure) in experimental buffer, followed by 10 minutes of incubation. The measurements were initiated 15 min after introducing protein. For each flow cell more than 200 beads were measured at a temperature of 25°C.

Electrophoretic mobility shift assay

The assay was performed on an AT-rich 200 bp DNA substrate (31% GC). DNA (25 ng) was incubated with different concentrations of the desired combination of MvaT, MvaT F36D/M44D and Mip in the binding buffer (10 mM Tris-HCl, 60 mM KCl, pH 8.0). The mixture was loaded on a 1% agarose gel (containing 1:104 dilution of Gel red DNA stain) with loading buffer (10 mM Tris-HCl, pH 7.6, 0.03% bromophenol blue, 0.03 % xylene cyanol FF, 60% glycerol and 60 mM EDTA). The samples were run at 4°C in TAE standard buffer. The gels were visualized with a Bio-rad Gel Doc XR+ system.

Isothermal Titration Calorimetry

Isothermal Titration Calorimetry experiments were performed as described previously (see Chapter 2) [13] with modifications. Briefly, ITC experiments were performed using a MicroCal VP-ITC system at 20 °C. The protein samples were dialyzed to a buffer containing 20 mM Bis-Tris, pH 6, 50 mM KCl, 16 mM $MgCl_2$. Typically, 20 µM of MvaT F36D/M44D was placed in the cell (1.4 ml) and titrated with 300 µM (500 µl) of the Mip, injected in 2 µl aliquots. The delay time between the injections was 60 s with a stirring speed of 307 rpm. The corresponding "protein to buffer" controls were performed for background correction. The ITC titration data were analysed using

Origin 7.0 (OriginLab) provided with the instrument. Standard deviation was calculated from the fit by Origin.

Bridging assay

The bridging assay was performed as described previously (see Chapter 2) [13] with modifications. To start the bridging reaction, MvaT was added, followed by 2 μl of Mip to different final concentrations. The samples were incubated while shaking at 1000 rpm at 25°C. The reactions were stopped and washed at certain time with buffer (10 mM Tris-HCl, pH 8, 65 mM KCl, 5% glycerol, 1 mg/ml BSA(ac), 1 mM spermidine, 20 mM $CaCl_2$, 0.02% Tween 20), followed by resuspension in 12 μl denaturing buffer (10 mM tris pH 8, 200 mM NaCl, 1 mM EDTA, 0.2% SDS (10%)). Scintillation was used to determine the final radioactivity of each sample. 2 μl of radioactive DNA was used as a reference to calculate the bridging efficiency (DNA recovery %).

NMR titration

The NMR titration of the MvaT dimer with Mip was performed on a 150 μM ^{15}N isotopically labelled protein sample, in 20 mM Bis-Tris Buffer, 50 mM KCl, 16 mM $MgCl_2$, pH 6 and 6% D_2O. A series of ^{1}H-^{15}N HSQC spectra were acquired by gradually increasing the Mip:MvaT molar ratio from 0.2 to 1.2. The experiments were recorded at 20 °C on a Bruker Avance III (HD) 600 MHz spectrometer, equipped with TCI cryoprobe, processed by TopSpin 3.5 (Bruker Biospin) and analysed by Sparky software [45]. The changes in peak positions and intensities were analysed by an in-house python script and the average chemical shift perturbations (CSP) were calculated using equation (1):

$$\Delta\delta_{avg} = \sqrt{\Delta\delta_H^2 + \frac{\Delta\delta_N^2}{6.25^2}} \qquad (1)$$

Modelling

The prediction of Mip 3D structure was performed using an *Ab initio* Rosetta modelling approach implemented in Robetta server (http://new.robetta.org). Prediction of the Mip-MvaT$_2$ complex was performed by HADDOCK2.2 server (https://milou.science.uu.nl/services/HADDOCK2.2) [35] using default setting parameters. The data from the NMR titration of the MvaT dimer with Mip was used to restrain the docking. The best *ab initio* model of Mip and the homology model of MvaT dimer

(see Chapter 2) [13] were used. Only the amino acids of site 1 of the MvaT dimer were classified as *active* in the docking settings. As no experimental information is available on which residues of Mip are involved in the complex formation, the full protein amino acid sequence was classified as *active*. Amino acid residues indirectly involved in complex formation (passive residues) were automatically identified by the server. HADDOCK clustered 138 structures in 16 clusters, which represents 69.0 % of the water-refined models HADDOCK generated. The statistics of the top cluster are shown in the table below. The top cluster is the most reliable according to HADDOCK. The reported scores and energies are averages calculated over the top four members of a cluster. The HADDOCK score is defined as: HADDOCK-score = $1.0*E_{VDW}+0.2*E_{ELEC}+1.0*E_{Desolvation}$

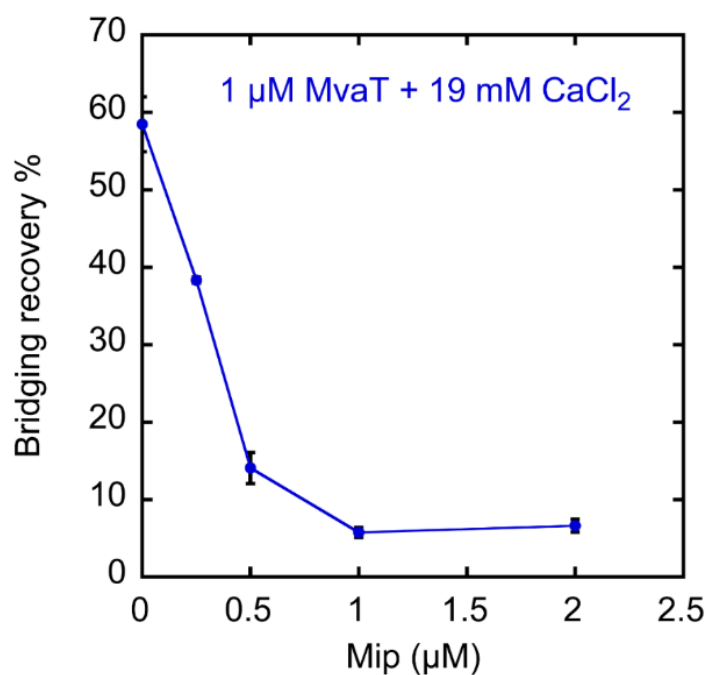| Cluster 3	
HADDOCK score	-103.3 +/- 14.3
Cluster size	11
RMSD from the overall lowest-energy structure	1.0 +/- 0.6
Van der Waals energy	67.0 +/- 7.6
Electrostatic energy	-360.2 +/- 63.5
Desolvation energy	-5.0 +/- 7.0
Restraints violation energy	407.9 +/- 78.85
Buried Surface Area	2369.2 +/- 90.2
Z-Score	-2.0

Supplementary information

Figure S3.1. **Mip inhibits the formation of a bridged DNA-MvaT-DNA complex.** DNA bridging efficiency (as a percentage of the input DNA) of MvaT (2.4 µM) as affected by titration of Mip at concentrations from 0 to 2.5 µM as measured by the DNA bridging pull down assay in the presence of 19 mM $CaCl_2$.
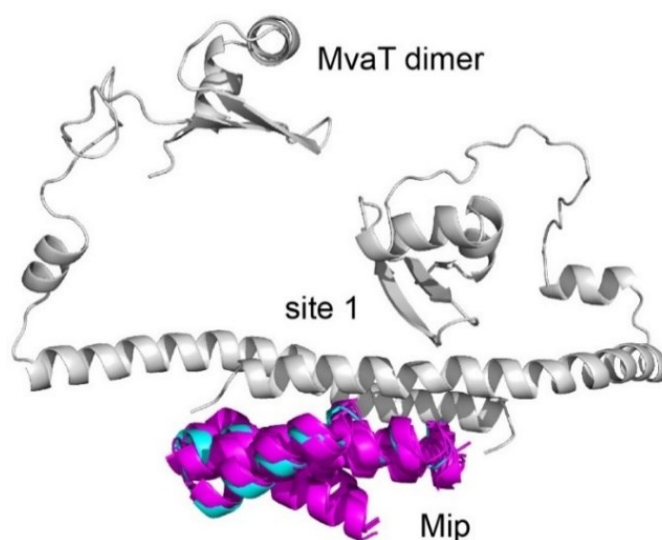

Figure S3.2: **HADDOCK best cluster of Mip-MvaT$_2$ complex**. The different orientations of Mip are shown in magenta cartoon and MvaT dimer in grey cartoon. The lowest energy structure of Mip within the complex is shown is cyan cartoon.

References

1   Bergh, O., Borsheim, K. Y., Bratbak, G. & Heldal, M. High abundance of viruses found in aquatic environments. *Nature* **340**, 467-468, doi:10.1038/340467a0 (1989).

2   Wommack, K. E. & Colwell, R. R. Virioplankton: viruses in aquatic ecosystems. *Microbiol. Mol. Biol. Rev.* **64**, 69-114, doi:10.1128/mmbr.64.1.69-114.2000 (2000).

3   Stern, A. & Sorek, R. The phage-host arms race: shaping the evolution of microbes. *Bioessays* **33**, 43-51, doi:10.1002/bies.201000071 (2011).

4   Chibani-Chennoufi, S., Bruttin, A., Dillmann, M.-L. & Brüssow, H. Phage-Host Interaction: an Ecological Perspective. *J. Bacteriol.* **186**, 3677, doi:10.1128/JB.186.12.3677-3686.2004 (2004).

5   Stone, E., Campbell, K., Grant, I. & McAuliffe, O. Understanding and Exploiting Phage-Host Interactions. *Viruses* **11**, 567, doi:10.3390/v11060567 (2019).

6   Enikeeva, F. N., Severinov, K. V. & Gelfand, M. S. Restriction-modification systems and bacteriophage invasion: who wins? *J. Theor. Biol.* **266**, 550-559, doi:10.1016/j.jtbi.2010.07.006 (2010).

7   Dupuis, M. E., Villion, M., Magadan, A. H. & Moineau, S. CRISPR-Cas and restriction-modification systems are compatible and increase phage resistance. *Nat Commun* **4**, 2087, doi:10.1038/ncomms3087 (2013).

8   Pfeifer, E., Hünnefeld, M., Popa, O. & Frunzke, J. Impact of Xenogeneic Silencing on Phage–Host Interactions. *J. Mol. Biol.*, doi:https://doi.org/10.1016/j.jmb.2019.02.011 (2019).

9   Flores-Rios, R., Quatrini, R. & Loyola, A. Endogenous and Foreign Nucleoid-Associated Proteins of Bacteria: Occurrence, Interactions and Effects on Mobile Genetic Elements and Host's Biology. *Comput Struct Biotechnol J* **17**, 746-756, doi:10.1016/j.csbj.2019.06.010 (2019).

10   Navarre, W. W. The Impact of Gene Silencing on Horizontal Gene Transfer and Bacterial Evolution. *Adv. Microb. Physiol.* **69**, 157-186, doi:10.1016/bs.ampbs.2016.07.004 (2016).

11   Huttener, M., Paytubi, S. & Juarez, A. Success in incorporating horizontally transferred genes: the H-NS protein. *Trends Microbiol.* **23**, 67-69, doi:10.1016/j.tim.2014.12.009 (2015).

12   Singh, K., Milstein, J. N. & Navarre, W. W. Xenogeneic Silencing and Its Impact on Bacterial Genomes. *Annu. Rev. Microbiol.* **70**, 199-213, doi:10.1146/annurev-micro-102215-095301 (2016).

13   Qin, L. *et al.* Structural basis for osmotic regulation of the DNA binding properties of H-NS proteins. *Nucleic Acids Res.*, doi:10.1093/nar/gkz1226 (2020).

14   Qin, L., Erkelens, A. M., Ben Bdira, F. & Dame, R. T. The architects of bacterial DNA bridges: a structurally and functionally conserved family of proteins. *Open Biol* **9**, 190223, doi:10.1098/rsob.190223 (2019).

15   Navarre, W. W., McClelland, M., Libby, S. J. & Fang, F. C. Silencing of xenogeneic DNA by H-NS-facilitation of lateral gene transfer in bacteria by a defense system that recognizes foreign DNA. *Genes Dev.* **21**, 1456-1471, doi:10.1101/gad.1543107 (2007).

16   Castang, S., McManus, H. R., Turner, K. H. & Dove, S. L. H-NS family members function coordinately in an opportunistic pathogen. *Proc Natl Acad Sci U S A* **105**, 18947-18952, doi:10.1073/pnas.0808215105 (2008).

17   Gordon, B. R., Imperial, R., Wang, L., Navarre, W. W. & Liu, J. Lsr2 of Mycobacterium represents a novel class of H-NS-like proteins. *J. Bacteriol.* **190**, 7052-7059, doi:10.1128/jb.00733-08 (2008).

18   Smits, W. K. & Grossman, A. D. The transcriptional regulator Rok binds A+T-rich DNA and is involved in repression of a mobile genetic element in Bacillus subtilis. *PLoS Genet.* **6**, e1001207, doi:10.1371/journal.pgen.1001207 (2010).

19   van der Valk, R. A. *et al.* Mechanism of environmentally driven conformational changes that modulate H-NS DNA-bridging activity. *Elife* **6**, doi:10.7554/eLife.27369 (2017).

20   Winardhi, R. S. *et al.* Higher order oligomerization is required for H-NS family member MvaT to form gene-silencing nucleoprotein filament. *Nucleic Acids Res.* **40**, 8942-8952, doi:10.1093/nar/gks669 (2012).

21   Qu, Y., Lim, C. J., Whang, Y. R., Liu, J. & Yan, J. Mechanism of DNA organization by Mycobacterium tuberculosis protein Lsr2. *Nucleic Acids Res.* **41**, 5263-5272, doi:10.1093/nar/gkt249 (2013).

22   Qin, L., Erkelens, A. M., Markus, D. & Dame, R. T. The B. subtilis Rok protein compacts and organizes DNA by bridging. *bioRxiv*, 769117, doi:10.1101/769117 (2019).

23   Liu, Q. & Richardson, C. C. Gene 5.5 protein of bacteriophage T7 inhibits the nucleoid protein H-NS of Escherichia coli. *Proc Natl Acad Sci U S A* **90**, 1761-1765, doi:10.1073/pnas.90.5.1761 (1993).

24   Ali, S. S., Beckett, E., Bae, S. J. & Navarre, W. W. The 5.5 protein of phage T7 inhibits H-NS through interactions with the central oligomerization domain. *J. Bacteriol.* **193**, 4881-4892, doi:10.1128/jb.05198-11 (2011).

25   Zhu, B., Lee, S. J., Tan, M., Wang, E. D. & Richardson, C. C. Gene 5.5 protein of bacteriophage T7 in complex with Escherichia coli nucleoid protein H-NS and transfer RNA masks transfer RNA priming in T7 DNA replication. *Proc Natl Acad Sci U S A* **109**, 8050-8055, doi:10.1073/pnas.1205990109 (2012).

26   Ho, C. H., Wang, H. C., Ko, T. P., Chang, Y. C. & Wang, A. H. The T4 phage DNA mimic protein Arn inhibits the DNA binding activity of the bacterial histone-like protein H-NS. *J. Biol. Chem.* **289**, 27046-27054, doi:10.1074/jbc.M114.590851 (2014).

27   Kano, Y., Yasuzawa, K., Tanaka, H. & Imamoto, F. Propagation of phage Mu in IHF-deficient Escherichia coli in the absence of the H-NS histone-like protein. *Gene* **126**, 93-97, doi:10.1016/0378-1119(93)90594-s (1993).

28   van Ulsen, P., Hillebrand, M., Zulianello, L., van de Putte, P. & Goosen, N. Integration host factor alleviates the H-NS-mediated repression of the early promoter of bacteriophage Mu. *Mol. Microbiol.* **21**, 567-578, doi:10.1111/j.1365-2958.1996.tb02565.x (1996).

29   Skennerton, C. T. *et al.* Phage Encoded H-NS: A Potential Achilles Heel in the Bacterial Defence System. *PLOS ONE* **6**, e20095, doi:10.1371/journal.pone.0020095 (2011).

30   Wagemans, J. *et al.* Antibacterial phage ORFans of Pseudomonas aeruginosa phage LUZ24 reveal a novel MvaT inhibiting protein. *Frontiers in Microbiology* **6**, 1242, doi:10.3389/fmicb.2015.01242 (2015).

31   Castang, S. & Dove, S. L. High-order oligomerization is required for the function of the H-NS family member MvaT in Pseudomonas aeruginosa. *Mol. Microbiol.* **78**, 916-931 (2010).

32   Dame, R. T. *et al.* DNA bridging: a property shared among H-NS-like proteins. *J. Bacteriol.* **187**, 1845-1848, doi:10.1128/jb.187.5.1845-1848.2005 (2005).

33   van der Valk, R. A., Qin, L., Moolenaar, G. F. & Dame, R. T. Quantitative Determination of DNA Bridging Efficiency of Chromatin Proteins. *Methods Mol Biol* **1837**, 199-209, doi:10.1007/978-1-4939-8675-0_12 (2018).

34   Bradley, P., Misura, K. M. & Baker, D. Toward high-resolution de novo structure prediction for small proteins. *Science* **309**, 1868-1871, doi:10.1126/science.1113801 (2005).

35   van Zundert, G. C. P. *et al.* The HADDOCK2.2 Web Server: User-Friendly Integrative Modeling of Biomolecular Complexes. *J. Mol. Biol.* **428**, 720-725, doi:10.1016/j.jmb.2015.09.014 (2016).

36   Drozdetskiy, A., Cole, C., Procter, J. & Barton, G. J. JPred4: a protein secondary structure prediction server. *Nucleic Acids Res.* **43**, W389-394, doi:10.1093/nar/gkv332 (2015).

37   van der Valk, R. A., Vreede, J., Cremazy, F. & Dame, R. T. Genomic looping: a key principle of chromatin organization. *J. Mol. Microbiol. Biotechnol.* **24**, 344-359, doi:10.1159/000368851 (2014).

38   Stoebel, D. M., Free, A. & Dorman, C. J. Anti-silencing: overcoming H-NS-mediated repression of transcription in Gram-negative enteric bacteria. *Microbiology* **154**, 2533-2545, doi:10.1099/mic.0.2008/020693-0 (2008).

39   Williamson, H. S. & Free, A. A truncated H-NS-like protein from enteropathogenic Escherichia coli acts as an H-NS antagonist. *Mol. Microbiol.* **55**, 808-827, doi:10.1111/j.1365-2958.2004.04421.x (2005).

40   Boudreau, B. A. *et al.* StpA and Hha stimulate pausing by RNA polymerase by promoting DNA–DNA bridging of H-NS filaments. *Nucleic Acids Res.* **46**, 5525-5546, doi:10.1093/nar/gky265 (2018).

41   Kotlajich, M. V. *et al.* Bridged filaments of histone-like nucleoid structuring protein pause RNA polymerase and aid termination in bacteria. *eLife* **4**, e04970, doi:10.7554/eLife.04970 (2015).

42   Ali, S. S. *et al.* Structural insights into the regulation of foreign genes in Salmonella by the Hha/H-NS complex. *J. Biol. Chem.* **288**, 13356-13369, doi:10.1074/jbc.M113.455378 (2013).

43   Ueda, T. *et al.* Functions of the Hha and YdgT proteins in transcriptional silencing by the nucleoid proteins, H-NS and StpA, in Escherichia coli. *DNA Res.* **20**, 263-271, doi:10.1093/dnares/dst008 (2013).

44   Gibson, D. G. *et al.* Enzymatic assembly of DNA molecules up to several hundred kilobases. *Nat. Methods* **6**, 343-345, doi:10.1038/nmeth.1318 (2009).

45   Lee, W., Tonelli, M. & Markley, J. L. NMRFAM-SPARKY: enhanced software for biomolecular NMR spectroscopy. *Bioinformatics* **31**, 1325-1327, doi:10.1093/bioinformatics/btu830 (2015).